Numerical Study on the Convective Heat Transfer Performance of a Developed MXene IoNanofluid in a Horizontal Tube by Considering Temperature-Dependent Properties

Meisam Ansarpour[a], Navid Aslfattahi[b,c], Masoud Mofarahi[a,*], R. Saidur[d,e]

[a]*Department of Chemical Engineering, Faculty of Petroleum, Gas and Petrochemical Engineering, Persian Gulf University, Bushehr,75169, Iran*

[b]*Department of Fluid Mechanics and Thermodynamics, Faculty of Mechanical Engineering, Czech Technical University in Prague, Technická 4, 160 00, Prague, Czech Republic*

[c]*Faculty of Mechanical Engineering, University of Tabriz, Tabriz 51666-16471, Iran*

[d]*Research Center for Nano-Materials and Energy Technology (RCNMET), School of Engineering and Technology, Sunway University, Bandar Sunway, Petaling Jaya, 47500, Selangor Darul Ehsan, Malaysia*

[e]*Department of Engineering, Lancaster University, Lancaster, LA1 4YW, UK*

ABSTRACT

In this study, the heat transfer performance of [MMI][DMP] ionic liquid solution (20 vol% IL + 80 vol% deionized water) in the presence of Mxene nanoparticle is investigated based on computational fluid dynamics numerical method considering temperature-dependent properties. It should be noted that the thermophysical properties of IoNanofluid were experimentally measured in our previous published study. The modeling results are validated with numerical and experimental works, and the validation results indicate good agreement between them. The effect

* Corresponding author: Masoud Mofarahi
Email: mofarahai@pgu.ac.ir

of adding Mxene nanoparticle to the base liquid was carried out in a horizontal tube with 1-50 range of Reynolds number. The results found that the heat transfer coefficient increased by increasing the Reynolds number and also the nanofluids' concentration. Moreover, it raises by increasing the fluid inlet temperature while the Nu number decreases. This is because the Nusselt number is in a reverse relationship with the heat transfer coefficient. The maximum heat transfer coefficient observed for 0.2 wt% INf at 308 K fluid inlet temperature and Reynolds number of 50 was 2207.83 W m^2 K^{-1}. However, the maximum Nusselt number detected for pure base fluid at 298.15 K fluid inlet temperature and Reynolds number of 50 which was 13.22. Furthermore, the maximum heat transfer enhancement was observed for 0.2 wt% INf at Reynolds number of 50 and 308.15 K fluid inlet temperature (43.6%). Finally, a novel correlation is proposed to estimate the Nusselt number of nanofluids with R^2=0.992 and AREP=2.8%.

Keywords - MXene - Ionic Liquid - Nanofluid – Heat Transfer - [Mmim][DMP] – Numerical Study

1. INTRODUCTION

Nowadays, nanofluids (Nfs) and nanoparticles (Nps) are widely used in industries such as paint, ceramic, food industries, etc. [1, 2]. Choi and Eastman [3] are the first pioneers who employed Nps as an additive in a base liquid to enhance thermal conductivity. They observed impressive results that encouraged other researchers to focus on these nanoscale materials [3].

It is known that ionic liquids (ILs) are organic salts with low melting points (<100 °C), which may be an alternative to traditional organic and inorganic solvents. ILs possess higher moisture

stability, thermal stability, solvating ability, and ionic conductivity. They also possess low vapor pressure which makes them a good candidate for solar applications [4, 5]. Moreover, ILs are non-volatile and nonflammable under ambient conditions and they are also considered green fluids due to their recyclability [6]. Researchers have also been interested in room-temperature ionic liquids (RTILs) because of their remarkable low melting points (<30 °C) which extends their usage in a wide range of applications [7].

On one hand, researchers are trying to enhance the IL's thermophysical properties via various methods like the addition of nanoparticles or mixing them with other solutions like water. For instance, Bridges et al. [8] studied the thermal properties of $[C_4mmim][NTf_2]$ IL in the presence of alumina and carbon black Nps. They reported that adding Al_2O_3 Nps to the IL increased the specific heat capacity; however, it decreased when adding carbon black. Wang et al. [9] studied the thermophysical properties of IoNanofluids (INfs) with Au Nps experimentally and theoretically. They reported that the viscosity of the base fluid plays a significant role in the thermal behavior of the INf [9]. Another study by Wang et al. [10] investigated the thermal conductivity of $[HMIM][BF_4]$ IL when Graphene or MWCNT INfs were present. They observed that the thermal conductivity of INfs increased slightly, compared to the base liquid. They also found out that the temperature does not affect the thermal conductivity [10]. Patil et al. [11] studied the density of some ILs and INfs of Ru Nps at temperatures between 20-70 °C. They observed that the density does not reduce significantly when adding Ru Nps to the IL which is not common [11].

On the other hand, several research groups have focused on increasing heat transfer efficiency by using INfs to enhance convective and natural heat transfer in engineering and

industrial systems. Paul et al. [12] investigated the natural convection of Al_2O_3/[C_4mpyrr][NTf_2] IL with 0.5, 1.0, and 2.5 wt.% concentrations in a rectangular enclosures. Their results showed the heat transfer coefficient (HTC) decreased even though thermophysical properties increased by adding Nps to the base liquid. That can be due to the relative enhancement in thermophysical properties, which are not sufficient to influence the natural convection of INfs. Besides, the interaction between solid particles and fluid and the accumulation of nanoparticles affect the heat transfer phenomenon [12]. Chereches et al. [13] numerically investigated the water-based alumina Nf in the presence of the [C_2mim][CH_3SO_3] IL in laminar flow. By adding 75 wt.% water to the pure IL, they concluded that the HTC decreased to 70% at minimum. They also reported that increasing *Re* number from 500 to 2000, increased the HTC to about 13%. Furthermore, the HTC of the INf was raised to 50% by adding 15wt.% alumina nanoparticles in the 0.25 water + 0.75 IL mixture, primarily because of the increment in the thermal conductivity and viscosity [13]. Ansarpour et al. [14] studied the effect of various factors on a heat transfer convection of [EMIM][$EtSo_4$] IL, ethylene glycol, and water as base fluids in the presence of Al_2O_3 nanoparticles. They also investigated the effect of fluid inlet temperature on heat transfer performance. They observed an increase in fluid inlet temperature led to a rise in HTC of water-based Nf. However, the HTC of ethylene glycol and IL-based Nfs decreased [14].

Unlike the previous studies which surveyed the various types of tubes such as tubes with twisted-tape inserts and dimple arrays and circular corrugated tubes, the present experimental work provides exciting results with MXene nanoparticles [15-18]. Computational fluid dynamics (CFD) is used to study the convective heat transfer in a horizontal tube with constant heat flux in this study. For the first time, the [Mmim][DMP] IL and Ti_3C_2 are used as the base fluid and Np,

respectively. The thermophysical properties of INf have been experimentally measured and published in our previous work for different concentrations (0.05, 0.1, and 0.2 wt.%) [19]. In addition to the other usual factors such as Reynolds (*Re*) number and Nfs concentration, the fluid inlet temperature is another factor studied here. The currently available correlations to predict the thermophysical properties of Nfs are almost exclusively for water-based Nfs, so it is essential to investigate convective heat transfer in INfs and provide good correlations to estimate the thermophysical properties of INfs. Therefore, the novel correlations for the base fluid and Nf thermophysical properties propose using experimental data obtained in this work.

2. MATERIALS AND METHODS

1,3-Dimethylimidazolium dimethyl-phosphate ionic liquid, [Mmim][DMP] was purchased from Merck KGaA, Darmstadt, Germany. **Tables (1)** and **(2)** represent the thermophysical properties of [Mmim][DMP] IL and MXene nanoparticle, respectively. No further purification has been done during the sample preparation. Highly purified deionized water (Purity ≥ 99.998%) was prepared at Research Centre for Nano Materials and Energy Technology (RCNMET), Sunway University, Malaysia. IL aqueous solution is precisely dispersed with Ti_3C_2 nanoparticles to produce Nf samples. To achieve this, IL aqueous solution was prepared by dissolving 20 vol.% of [Mmim][DMP] into 80 vol.% of deionized water by magnetic stirring for 30 minutes at 45ºC and 700 rpm to obtain a homogenous mixture. The detailed experimental results and preparation method are presented in our previous published research study [19].

Table 1

Table 2

2.1 Thermophysical correlations

The base fluid's and Nf's temperature-dependent properties were optimized by MINITAB 16.2.0 using Polynomial Regression Analysis via Guess-Newton algorithm. The results were highly accurate and are reported in **Table 3**.

Table 3

Figures (1-4) compare the experimental results published in our previous paper [19] and those obtained by the empirical correlations.

Figure (1)

Figure (2)

Figure (3)

Figure (4)

2.2 Methodology

The governing equations (continuity, momentum, and energy) are reported in **Equations (1-3)** [20].

$$\nabla.(\rho\vec{V}) = 0 \tag{1}$$

$$\nabla.(\rho\vec{V}\vec{V}) = -\nabla(P) + \nabla.(\mu\nabla\vec{V}) \tag{2}$$

$$\nabla.(\rho\vec{V}C_pT) = \nabla.(K\nabla T) \tag{3}$$

To calculate the local and average heat transfer coefficients, respectively **Equations (4)** and **(5)** were employed.

$$h_x = \frac{q}{[T_w - T_b]_x} \tag{4}$$

$$h_{avg} = \frac{1}{L}\int_0^L h_x dx \tag{5}$$

Nu number was calculated using the following equation:

$$Nu = \frac{hD_h}{k} \tag{6}$$

2.3 Problem statement

CFD analyses are widely used to simulate experiments due to experiment limitations such as the cost of investigations and time consumption. The finite volume method has been

employed to solve the governing equations (momentum, mass, and energy equations) in the Fluent 16.2 software because of its higher accuracy than the finite element method. SIMPLEC algorithm and the second-order upwind discretization with a maximum residual value of 1E-05 [21, 22] were used to solve the pressure velocity coupling and discretize the governing equations, respectively [23, 24]. Several researchers compared the single-phase and multiphase methods and reported that the single-phase is more suitable for low concentrations of Nfs due to the consumption of less computation [6, 25-27]. Besides, using the experimental thermophysical properties will reduce the error of using the single-phase approach compared to the multiphase approach. Note that, interactions between particles and base fluid, (e.g. Brownian molecular motion and thermo-phoretic forces) are not considered [28]. Nevertheless, the single-phase fluid was supposed to study the heat transfer of INf in this research.

2.4 Thermal boundary conditions

The boundary conditions of this study are: inlet, velocity inlet; outlet, pressure outlet; wall, uniform heat flux. The analyses were based on single-phase assumption and thermal boundary conditions as follows:

1) steady-state, Laminar, and 2-D.
2) The mass fraction of nanoparticles is varied from 0 to 0.2%.
3) All tests are made for a *Re* range of 1-50.
4) A uniform heat flux on the wall = 3000 W m^{-2}.
5) The fluid inlet temperature varies from 298.15 K to 308.15 K.
6) Thermophysical properties of the fluid change with temperature (**Table (3)**).

2.5 Geometry, meshing, and grid independence

Figures (5) and **(6)** show the computational domain studied in this work and its mesh, which is a horizontal tube with 4.0 mm diameter and 6.0 m length.

Figure 5

Figure 6

A grid validation was performed for the computational domain to find the optimum mesh grids. The results are available in Table (4). The grid independence test is carried out for configuring horizontal tube to ensure the reliability of the numerical results. The mesh structure consists of rectangular mesh elements as shown in figure 6. Accordingly, seven different grids are examined for the tested tube utilizing water as a working fluid and 3000 W m^2 heat flux, and the error percentage in terms of Nusselt number between grid numbers is calculated. It was observed that there was no further change in Nu_{avg} after mesh no. 6 and it was detected that the REP was 0.61% as shown in Table 4. It is not useful to grow the number of cells to more than 18000 hence the grid number of 18000 is accepted for the processing of the tests remainder in the current study. As far as quality measures are concerned, we checked the orthogonal and skewness of the elements and the values were 1.4317E-02 (Minimum: 1.3057E-02, Maximum:

2.0289E-01, Average: 1.4317E-02) and 1.0, respectively. These values give us good quality mesh.

Moreover, the error percent in the **table (4)** is calculated from Equation (7):

$$REP = \frac{|Nu_{old} - Nu_{new}|}{Nu_{new}} \times 100 \quad (7)$$

Table 4

2.6 Model validation

One of the critical steps for numerical analysis is to validate the numerical model by comparing the simulation results with known experimental or theoretical results. The model was validated with both practical and numerical works at 298.15 K fluid inlet temperature, 3000 W m^{-2} heat flux, *Re*=1800, and pure water. **Figure (7)** shows the model validation by reporting Nu_x. It is clear from **Figure (7)** that there is a good agreement between the results from this study with Sajjad et al. [29], with an accuracy of about 3.65% AREP (numerical research), and Meyer and Everts [30] with 13.3% AREP (experimental study). The first and second columns refer to the number of divisions in radial and axial directions, respectively.

Figure 7

The summary of key parameter is available in **Table (5)**:

Table (5)

3. RESULTS AND DISCUSSION

There are different mechanisms that affect the Nfs' performance such as thermal diffusion, persuaded micro convection, Brownian motion of the nanoparticles, decreased thermal boundary-layer thickness, increased conduction through accumulates, and liquid layering on the nanoparticle–liquid interface [31-33].

The *Nu* number and HTC of INfs compared to the pure IL are reported in the following sections. The effect of various factors such as Nfs concentration, fluid inlet temperature, and *Re* number on the HTC and *Nu* number are also presented.

3.1 The effect of *Re* number variation on the *Nu* and the HTC

Figures (8) and **(9)** show the HTC and *Nu* numbers of INfs with different concentrations versus *Re* numbers. It is clear *Re* number affects the thermal performance [34]. As shown in **Figure (8)**, HTC increases by increasing the *Re* number for all concentrations of Nfs. The higher value of the *Re* has a positive effect on the heat transfer coefficient. So, the Nfs may perform better at higher *Re*. This statement is in agreement with the results presented by other researchers [35-37]. This can be as a result of an increment in the fluid inlet velocity which has a noticeable influence on the HTC [36].

Figure 8

In addition, **Figure (9)** indicates that *Nu* number will increase significantly by a rise in *Re* number at room temperature. According to Equation (6), it is clear that when HTC increases, *Nu* number will grow too. The same results were reported by the other researchers [38-42]. The increment in Nu number can be due to an increase in fluid velocity which decreases the thickness of the boundary layer and then the heat transfer coefficient and Nu number rise [43, 44].

Figure 9

3.2 The effect of Nfs concentration on the HTC and the *Nu* number

The concentration of Nfs is a significant factor that influences their behavior. It is described as the ratio of the mass (or volume) of nanoparticles to the base fluid. As expected, Nps concentration plays an important role in thermal conductivity (and heat transfer) since Nps have higher thermal conductivity than base fluids.

Adding nanoparticles to the base fluid decreases the temperature difference between the heated wall and the bulk fluid which results in a higher heat transfer performance [28]. Previous studies considered the influence of Nf concentration and reported similar results. They observed that a rise in Nf concentration improves the heat transfer process [35, 36]. In most cases, the viscosity of the base fluids increases after adding nanoparticles to them [45, 46].

Figures (10) and **(11)** show the *Nu* number and heat transfer coefficient variation for different *Re* numbers at 298.15 K. As shown in **Figure (10),** HTC increases by increasing Nfs concentration, and maximum HTC is observed for INf with 0.2 wt.% at *Re*=50. Different

numerical and experimental researches have confirmed that an increase in Nfs concentration leads to an increased HTC [47, 35, 48]. Ghozatloo et al. reported a 35.6% increment in HTC for water-based graphene Nfs at 0.1 wt.% Nfs concentration [49]. Arzani et al. observed 22% enhancement in HTC and 0.1 wt.% for water-based GNP Nfs [50]. Generally, by adding Nps to the base fluid, the temperature difference between the heated wall and the bulk fluid decrease, consequently, the heat transfer performance will improve [28]. Moreover, the increment in HTC could be due to the role of thermal conductivity that is rising by growing the Nf's concentration [6].

Figure 10

However, the obtained results for the *Nu* number are different and no significant change has been observed at these volume fractions. By adding Nps to the base fluid at 0.05 wt.%, *Nu* number increased slightly, and increasing Nfs concentration leads to a negligible reduction in *Nu* number. It is also obvious in **Equation (6)** which indicates that the *Nu* number is in a reverse relationship with the thermal conductivity term. In turn, the thermal conductivity increases by increasing Nfs concentration [3, 10]. Maığa et al. [51] investigated the effect of adding nanoparticles to the water and ethylene glycol as base fluids in a horizontal tube and observed that heat transfer performance improved due to adding nanoparticles [51]. In other researches, Ajeel et al. [52-54] studied the thermal-hydraulic performance in a curved-corrugated channel model and reported that Nu number increased as a result of adding nanoparticles to the base fluid

[52-54]. However, Pakravan and Yaghoubi [55] also investigated the effect of Nfs concentration on the natural convection heat transfer in a cavity. They reported that the *Nu* number decreased by increasing Nps size and concentration [55].

According to Nfs concentration, viscosity and density are the two thermophysical properties that may affect the heat transfer performance, significantly. Therefore, increasing Nfs concentration without considering these two properties, may result in negative results in the heat transfer performance [47].

Figure 11

3.3 The effect of fluid inlet temperature

Fluid inlet temperature is likely one of the significant factors in the heat transfer phenomenon, which was not considered by prior researchers for INFS as it should have been. Fluid inlet temperature have been applied in the range of 298.15 to 308.15 K because of the limitations induced by the available correlations.

Figure (12), shows the HTC as a function of two important factors: fluid inlet temperature and *Re*=25. The results indicate that HTC will increase by increasing fluid inlet temperature. To discuss about the results in a good way, the properties that affected by temperature variations and consequently, affect the heat transfer performance are discussed in the following. This enhancement in HTC can be due to the increased thermal conductivity which happens when temperature rises. These observed results may be due to temperature fluctuations that change the

thermal conductivity of Nfs. Previously, thermal conductivity has been studied by different researchers as a thermophysical property of INfs [6, 11, 56]. França et al. [57] investigated the effect of MWCNT nanoparticles compared to the base fluid (IL) at different temperatures. Their results showed that the INFs thermal conductivity reduced when there was a rise in temperature [57]. Same results were reported by Ribeiro et al. [58]. Heat capacity is a property which has not been studied much in the presence of Nfs. Wang et al. [10] applied MWCNT and graphene [HMIM]BF_4 IL in their experiments and observed a minor enhancement of specific heat capacity when rising temperature. They also observed that there will be a negligible decrement in specific heat capacity due to the presence of nanoparticles [10]. Moreover, Paul et al. [12] studied the effects of INfs temperature and concentration on the specific heat of Al_2O_3 nanoparticles suspended in [C_4mpyrr][NTf_2] IL. They reported that specific heat of Nfs raised slightly by increasing temperature [12].

Heat transfer performance and practical thermal applications are also affected by viscosity. To increase the accuracy of researches, viscosity should be considered as a temperature-dependent property in the investigations. Temperature dependency of viscosity for [C_4mpyrr][NTf_2] IL-based INfs was studied by Paul et al. [59], and they observed that viscosity reduces by rising the fluid temperature [59].

All the mentioned properties and their temperature dependency affect the HTC and *Nu* number which is shown in **Figures (12)** and **(13)**.

Figure 12

Figure (13) presents the *Nu* number versus fluid inlet temperature at *Re* = 25. As shown *Nu* number at all studied concentrations of INfs decreases when increasing temperature. The same result reported by Ansarpour et al. [14]. They observed that *Nu* number of Nfs (based on [EMIM][$EtSO_4$] IL and Ethylene glycol) decreases by increasing temperature [14].

Figure 13

In the following, **Figure (14)** compares the HTC values calculated from **Eq. (4)** and two other experimental correlations (**Eqs. (8) [60] and (9) [48]**) to estimate HTC of nanofluids. First, *Nu* number calculated from **Eqs. (8)** and **(9)** and then HTC calculated using **Eq. (6)**. The figure is drawn for HTC values of INfs with 0.05 and 0.1 wt.% concentrations versus fluid inlet temperature. As shown in **Figure (14)**, there is an obvious difference between the results from **Eq. (4)** and the other correlations (AREPs for **Eq. (8)** = 16.8% and for **Eq. (9)** = 31.2%.) which could be due to some reasons such as: (1) different Np's type. (2) different *Re* range. (3) different working temperature. (4) different Nf's concentration.

$$Nu_{nf} = 0.4328(1+11.285\varphi^{0.754}Pe^{0.218})\,\mathrm{Re}^{0.333}\,\mathrm{Pr}^{0.4} \quad (8)$$

$$Nu_{nf} = 0.306\,\mathrm{Re}^{0.579}\,\mathrm{Pr}^{0.85}(1+\varphi)^{164.107}((1+\varphi)\,\mathrm{Re}_{np})^{0.002} \quad (9)$$

Figure 14

There is an evident lack of correlation to estimate HTC at low *Re* numbers and Nf's concentration. Moreover, there is no correlation to calculate the *Nu* or HTC of Mxene Nfs. Thus, the tolerance exists in **Figure (14)** is predictable.

3.4 The effect of various parameters on the heat transfer enhancement (HTE)

Figures (15) and **(16)** show the HTE of INfs compared to the base liquid. The values of HTE and HTC for IL are available in the primary vertical axis and the secondary one, respectively. As can be seen from the figures, HTE increased when the temperature increases. The maximum HTE was observed when 0.2 wt.% of INf was present at *Re*=1 and T= 308.15 K which was about 43.6%. Previous researches reported that HTC could be increased by more than 20% as a result of using Nfs, even at low concentrations (< 5 vol.%) [47, 61]. The same results were observed by Meisam et al. [48]. They argued that using INfs in lower *Re* is influential since the induced microconvection effect on the convective heat transfer enhancement is prominent at low *Re* numbers [48].

Figure 15

As can be seen from **Figure (16)**, HTE doesn't show the significant change (slightly reduction) by increasing *Re* number. The same results were reported by Minea and Murshed [6], the author

didn't observe that by adding 1% of MWCNT to [C_4mim][NTf_2] and [C_2mim][$EtSO_4$] ionic liquids, the HTE remains almost constant with Re variation in the laminar flow [6].

This phenomenon can be explained by the combined influence of an increase in thermal conductivity and viscosity of the base liquid in presence of Nps. Moreover, it could depend on the role of anions and cations of IL dissociate when blended with a polar fluid (water), creating dissociated ions. Thus, a description may rely on the formation of water molecules around IL ions correlated with the reduction of bonds between IL ionic components once water is added. On the other hand, the HTE is slightly reducing with *Re* number growth, which is acceptable for Nfs because of a simultaneous upsurge in both viscosity and thermal conductivity [6, 13, 62].

Figure 16

Furthermore, **Table (6)** compares the reported Nf's HTE of previous studies and this work.

Table 6

As mentioned in Table (6), a reduction in HTE is obvious. Paul et al. [12] claimed particle–fluid interaction and clustering of NPs also have a significant role in reducing the heat transfer

coefficient. They also believe the negative effect of enhanced viscosity in presence of Nps surpassed the enhancement of other thermophysical properties [12].

3.5 Proposed *Nu* correlation for studied Nfs

After all, a correlation has been proposed to estimate the *Nu* numbers of Nfs as a function of *Re*, *Pr* and Nf volume concentration (φ). The parameters are functions of the thermophysical properties, like heat capacity, density, thermal conductivity, and fluid viscosity. As shown in **Figure (17)**, the proposed correlation successfully modeled the system with 0.0, 0.05, 0.1, and 0.2 wt.% Nf's concentration under the laminar flow regime (Re=1-50) at the temperature range of 298.15 K to 308.15 K with R^2=0.992 and AREP=2.8%.

To estimate the Nu number of Nfs, the following equation was selected among all of the available correlations reported in the literature:

$$Nu_{nf} = a(\mathrm{Re}.\mathrm{Pr})^{b}(1+\varphi)^{c} \quad (10)$$

To optimize the correlation parameters, Minitab 16.2.0 software was applied by using the Gauss-Newton algorithm with a tolerance of 1E-05. The equation was correlated with R^2=0.992 and minimum, maximum, and average REP of 0.26%, 5.57%, and 2.8%, respectively. The obtained correlation was as follows:

$$Nu_{nf} = 2.96(\mathrm{Re}.\mathrm{Pr})^{0.231}(1+\varphi)^{9.7} \quad (11)$$

Moreover, **Figure (17)** shows the scatter plot for numerical *Nu* numbers versus predicted *Nu* numbers that indicate good agreement between predicted and model results within the maximum ±15% deviation range (the dash lines). Thus, the accuracy of the proposed correlation (**Eq. (11)**) is completely reliable to estimate the *Nu* number of INfs for the following ranges of the parameters: *Re* = 1-50; fluid inlet temperature = 298.15-308.15 K; INfs' concentration <=0.2 wt.%.

Figure 17

4. CONCLUSION

In this study, a horizontal tube was simulated to investigate the heat transfer performance for [Mmim][DMP] IL + water solution as a base fluid and Ti_3C_2 (MXene) as an additive. Its novelty is based on the original approach to implement experimental thermophysical properties of MXene nanoparticle in a convective heat transfer survey by considering temperature-dependent properties. Various *Re* numbers, fluid inlet temperature and concentrations are the factors studied in this research. The applied Nf's concentrations of IL are 0.05, 0.1 and 0.2 mass fractions. The results showed that HTC increased by increasing Nf's concentration and fluid inlet temperature; However, *Nu* number decreased. Note that, HTC and *Nu* numbers increased by increasing *Re* number. The maximum HTC was observed for 0.2 wt.% INf and maximum HTE at *Re*=50 and T=298.15 K and the maximum HTE observed by 0.2 wt.% INf at *Re*=1 and T=308.15 K, that are

2207.8 (W m^{-2} K^{-1}) and 43.6%, respectively. In other words, maximum HTC and HTE were observed at the maximum and minimum studied *Re* numbers, respectively. Finally, the correlations used for both base fluid and Nf thermophysical properties, presented by experimental data and the properties of the fluids were considered as the temperature-dependent properties in the modeling; Furthermore, a new correlation was proposed to estimate *Nu* number of INfs based on thermophysical properties and volume fraction. The results were in good agreement with the experimental data with an accuracy of R^2=0.992 and AREP=2.8%. For future researches, it is suggested to investigate various geometry with different applications and the other thermophysical properties of other ionic liquids.

FUTURE ASPECTS

INfs require further investigation to determine their thermophysical properties and heat transfer performance since the most important question to be addressed is the estimation of the thermophysical properties of INfs. Thus, there is a critical necessity in the study of INfs to get a view of the INfs possible applications as new heat transfer fluids. Besides, the lack of experimental thermophysical properties enforce the author to perform investigation only at low concentrations of Mxene INf as a novel nanoparticle in the heat transfer area.

DECLARATIONS

Conflict of interest: The authors have no conflicts of interest to declare that are relevant to the content of this article.

NOMENCLATURE

Latin symbols

c_p	specific heat capacity [J kg^{-1} $^oK^{-1}$]
D_h	hydraulic diameter of PHE [m]
K	thermal conductivity [W m^{-1} K^{-1}]
L	length of the tube [m]
Nu	Nusselt number
Pr	Prandtl number
Re	Reynolds number
wt.%	mass concentration

Greek symbols

μ	fluid viscosity [Pa.s]
ρ	fluid density [kg m^{-3}]
ϕ	volume concentration

Subscripts

bf	base fluid
h	hydraulic
nf	Nanofluid
np	Nanoparticle
w	Water

Abbreviations

AREP	average relative error percent
HTC	heat transfer coefficient [W m^{-2} K^{-1}]
IL	Ionic liquid
INf	IoNanofluid
REP	relative error percent

REFERENCES

1. F. Gibbs SK, Inteaz Alli, Catherine N. Mulligan, Bernard. Encapsulation in the food industry: a review. International journal of food sciences and nutrition. 1999;50(3):213-24.
2. Lewis JA. Colloidal processing of ceramics. Journal of the American Ceramic Society. 2000;83(10):2341-59.
3. Choi SU, Eastman JA. Enhancing thermal conductivity of fluids with nanoparticles: Argonne National Lab., IL (United States)1995.
4. Ngo HL, LeCompte K, Hargens L, McEwen AB. Thermal properties of imidazolium ionic liquids. Thermochimica Acta. 2000;357:97-102.
5. Welton T. Room-temperature ionic liquids. Solvents for synthesis and catalysis. Chemical reviews. 1999;99(8):2071-84.
6. Minea AA, Murshed SS. A review on development of ionic liquid based nanofluids and their heat transfer behavior. Renewable and Sustainable Energy Reviews. 2018;91:584-99.
7. Marsh K, Boxall J, Lichtenthaler R. Room temperature ionic liquids and their mixtures—a review. Fluid phase equilibria. 2004;219(1):93-8.
8. Bridges NJ, Visser AE, Fox EB. Potential of nanoparticle-enhanced ionic liquids (NEILs) as advanced heat-transfer fluids. Energy & Fuels. 2011;25(10):4862-4.
9. Wang B, Wang X, Lou W, Hao J. Ionic liquid-based stable nanofluids containing gold nanoparticles. Journal of colloid and interface science. 2011;362(1):5-14.
10. Wang F, Han L, Zhang Z, Fang X, Shi J, Ma W. Surfactant-free ionic liquid-based nanofluids with remarkable thermal conductivity enhancement at very low loading of graphene. Nanoscale research letters. 2012;7(1):314.
11. Patil V, Cera-Manjarres A, Salavera D, Rode C, Patil K, Nieto De Castro C et al. Ru-Imidazolium Halide IoNanofluids: Synthesis, Structural, Morphological and Thermophysical Properties. Journal of Nanofluids. 2016;5(2):191-208.
12. Paul TC, Morshed A, Fox EB, Khan JA. Experimental investigation of natural convection heat transfer of Al2O3 Nanoparticle Enhanced Ionic Liquids (NEILs). International Journal of Heat and Mass Transfer. 2015;83:753-61.
13. Cherecheş EI, Minea AA, Sharma K. A complex evaluation of [C2mim][CH3SO3]–alumina nanoparticle enhanced ionic liquids internal laminar flow. International Journal of Heat and Mass Transfer. 2020;154:119674.
14. Ansarpour M, Danesh E, Mofarahi M. Investigation the effect of various factors in a convective heat transfer performance by ionic liquid, ethylene glycol, and water as the base fluids for Al2O3 nanofluid in a horizontal tube: A numerical study. International Communications in Heat and Mass Transfer. 2020;113:104556.
15. Al-Obaidi AR, Chaer I. Study of the flow characteristics, pressure drop and augmentation of heat performance in a horizontal pipe with and without twisted tape inserts. Case Studies in Thermal Engineering. 2021;25:100964.
16. Al-Obaidi AR. Investigation of fluid field analysis, characteristics of pressure drop and improvement of heat transfer in three-dimensional circular corrugated pipes. Journal of Energy Storage. 2019;26:101012.
17. Al-Obaidi AR, Sharif A. Investigation of the three-dimensional structure, pressure drop, and heat transfer characteristics of the thermohydraulic flow in a circular pipe with different twisted-tape geometrical configurations. Journal of Thermal Analysis and Calorimetry. 2021;143(5):3533-58.
18. Al-Obaidi AR. Study the influence of concavity shapes on augmentation of heat-transfer performance, pressure field, and fluid pattern in three-dimensional pipe. Heat Transfer. 2021;50(5):4354-81.

19. Das L, Habib K, Saidur R, Aslfattahi N, Yahya SM, Rubbi F. Improved thermophysical properties and energy efficiency of aqueous ionic liquid/MXene nanofluid in a hybrid PV/T solar system. Nanomaterials. 2020;10(7):1372.
20. Bianco V, Chiacchio F, Manca O, Nardini S. Numerical investigation of nanofluids forced convection in circular tubes. Applied Thermal Engineering. 2009;29(17-18):3632-42.
21. Hosseinnezhad R, Akbari OA, Afrouzi HH, Biglarian M, Koveiti A, Toghraie D. Numerical study of turbulent nanofluid heat transfer in a tubular heat exchanger with twin twisted-tape inserts. Journal of Thermal Analysis and Calorimetry. 2018;132(1):741-59.
22. Alrashed AA, Akbari OA, Heydari A, Toghraie D, Zarringhalam M, Shabani GAS et al. The numerical modeling of water/FMWCNT nanofluid flow and heat transfer in a backward-facing contracting channel. Physica B: Condensed Matter. 2018;537:176-83.
23. Alikhani S, Behzadmehr A, Saffar-Avval M. Numerical study of nanofluid mixed convection in a horizontal curved tube using two-phase approach. Heat and mass transfer. 2011;47(1):107-18.
24. Khodabandeh E, Ghaderi M, Afzalabadi A, Rouboa A, Salarifard A. Parametric study of heat transfer in an electric arc furnace and cooling system. Applied Thermal Engineering. 2017;123:1190-200.
25. Albojamal A, Vafai K. Analysis of single phase, discrete and mixture models, in predicting nanofluid transport. International Journal of Heat and Mass Transfer. 2017;114:225-37.
26. Li Q, Xuan Y, editors. Convective heat transfer performances of fluids with nano-particles. International Heat Transfer Conference Digital Library; 2002: Begel House Inc.
27. Pak BC, Cho YI. Hydrodynamic and heat transfer study of dispersed fluids with submicron metallic oxide particles. Experimental Heat Transfer an International Journal. 1998;11(2):151-70.
28. Minea AA, Buonomo B, Burggraf J, Ercole D, Karpaiya KR, Di Pasqua A et al. NanoRound: A benchmark study on the numerical approach in nanofluids' simulation. International Communications in Heat and Mass Transfer. 2019;108:104292.
29. Sajjad M, Kamran MS, Shaukat R, Zeinelabdeen MIM. Numerical investigation of laminar convective heat transfer of graphene oxide/ethylene glycol-water nanofluids in a horizontal tube. Engineering science and technology, an international journal. 2018;21(4):727-35.
30. Meyer JP, Everts M. Single-phase mixed convection of developing and fully developed flow in smooth horizontal circular tubes in the laminar and transitional flow regimes. International Journal of Heat and Mass Transfer. 2018;117:1251-73.
31. Mohammed H, Al-Aswadi A, Shuaib N, Saidur R. Convective heat transfer and fluid flow study over a step using nanofluids: a review. Renewable and Sustainable Energy Reviews. 2011;15(6):2921-39.
32. Buongiorno J. Convective transport in nanofluids. Journal of heat transfer. 2006;128(3):240-50.
33. Krishnamurthy S, Bhattacharya P, Phelan P, Prasher R. Enhanced mass transport in nanofluids. Nano letters. 2006;6(3):419-23.
34. Al-Obaidi AR. Investigation of the flow, pressure drop characteristics, and augmentation of heat performance in a 3D flow pipe based on different inserts of twisted tape configurations. Heat Transfer. 2021;50(5):5049-79.
35. Tohidi A, Ghaffari H, Nasibi H, Mujumdar A. Heat transfer enhancement by combination of chaotic advection and nanofluids flow in helically coiled tube. Applied Thermal Engineering. 2015;86:91-105.
36. Togun H, Abu-Mulaweh HI, Kazi SN, Badarudin A. Numerical simulation of heat transfer and separation Al2O3/nanofluid flow in concentric annular pipe. International Communications in Heat and Mass Transfer. 2016;71:108-17.
37. Shalchi-Tabrizi A, Seyf HR. Analysis of entropy generation and convective heat transfer of Al2O3 nanofluid flow in a tangential micro heat sink. International Journal of Heat and Mass Transfer. 2012;55(15-16):4366-75.
38. Al-Obaidi AR. Investigation on effects of varying geometrical configurations on thermal hydraulics flow in a 3D corrugated pipe. International Journal of Thermal Sciences. 2022;171:107237.

39. Al-Obaidi AR, Alhamid J. Investigation of flow pattern, thermohydraulic performance and heat transfer improvement in 3D corrugated circular pipe under varying structure configuration parameters with development different correlations. International Communications in Heat and Mass Transfer. 2021;126:105394.
40. Al-Obaidi AR, Alhamid J, editors. Numerical investigation of fluid flow, characteristics of thermal performance and enhancement of heat transfer of corrugated pipes with various configurations. Journal of Physics: Conference Series; 2021: IOP Publishing.
41. Alhamid J, Al-Obaidi AR, editors. Effect of concavity configuration parameters on hydrodynamic and thermal performance in 3D circular pipe using Al2O3 nanofluid based on CFD simulation. Journal of Physics: Conference Series; 2021: IOP Publishing.
42. Alhamid J, Al-Obaidi RA, editors. Flow pattern investigation and thermohydraulic performance enhancement in three-dimensional circular pipe under varying corrugation configurations. Journal of Physics: Conference Series; 2021: IOP Publishing.
43. Al-Obaidi AR, Alhamid J, Hamad F. Flow felid and heat transfer enhancement investigations by using a combination of corrugated tubes with a twisted tape within 3D circular tube based on different dimple configurations. Heat Transfer. 2021;50(7):6868-85.
44. Al-Obaidi AR. Analysis of the flow field, thermal performance, and heat transfer augmentation in circular tube using different dimple geometrical configurations with internal twisted-tape insert. Heat Transfer. 2020;49(8):4153-72.
45. Murshed S, Leong K, Yang C. Thermophysical and electrokinetic properties of nanofluids–a critical review. Applied thermal engineering. 2008;28(17-18):2109-25.
46. Fox EB, Visser AE, Bridges NJ, Amoroso JW. Thermophysical properties of nanoparticle-enhanced ionic liquids (NEILs) heat-transfer fluids. Energy & Fuels. 2013;27(6):3385-93.
47. Vanaki SM, Ganesan P, Mohammed H. Numerical study of convective heat transfer of nanofluids: a review. Renewable and Sustainable Energy Reviews. 2016;54:1212-39.
48. Meisam A, Ahmad A, Hamed M. Experimental Investigation of Metal Oxide Nanofluids in a Plate Heat Exchanger. Journal of Thermophysics and Heat Transfer. 2019:1-12.
49. Ghozatloo A, Rashidi A, Shariaty-Niassar M. Convective heat transfer enhancement of graphene nanofluids in shell and tube heat exchanger. Experimental Thermal and Fluid Science. 2014;53:136-41.
50. Arzani HK, Amiri A, Kazi S, Chew B, Badarudin A. Experimental and numerical investigation of thermophysical properties, heat transfer and pressure drop of covalent and noncovalent functionalized graphene nanoplatelet-based water nanofluids in an annular heat exchanger. International Communications in Heat and Mass Transfer. 2015;68:267-75.
51. Maïga SEB, Nguyen CT, Galanis N, Roy G. Heat transfer behaviours of nanofluids in a uniformly heated tube. Superlattices and Microstructures. 2004;35(3):543-57.
52. Ajeel RK, Zulkifli R, Sopian K, Fayyadh SN, Fazlizan A, Ibrahim A. Numerical investigation of binary hybrid nanofluid in new configurations for curved-corrugated channel by thermal-hydraulic performance method. Powder Technology. 2021;385:144-59.
53. Ajeel RK, Sopian K, Zulkifli R. A novel curved-corrugated channel model: Thermal-hydraulic performance and design parameters with nanofluid. International Communications in Heat and Mass Transfer. 2021;120:105037.
54. Ajeel RK, Sopian K, Zulkifli R. Thermal-hydraulic performance and design parameters in a curved-corrugated channel with L-shaped baffles and nanofluid. Journal of Energy Storage. 2021;34:101996.
55. Pakravan HA, Yaghoubi M. Analysis of nanoparticles migration on natural convective heat transfer of nanofluids. International journal of thermal sciences. 2013;68:79-93.
56. De Castro CN, Murshed SS, Lourenço M, Santos F, Lopes M, França J. Enhanced thermal conductivity and specific heat capacity of carbon nanotubes ionanofluids. International Journal of Thermal Sciences. 2012;62:34-9.

57. França J, Vieira S, Lourenço M, Murshed S, Nieto de Castro C. Thermal conductivity of [C4mim][(CF3SO2) 2N] and [C2mim][EtSO4] and their ionanofluids with carbon nanotubes: experiment and theory. Journal of Chemical & Engineering Data. 2013;58(2):467-76.
58. Ribeiro A, Vieira S, Goodrich P, Hardacre C, Lourenço M, de Castro C. Thermal Conductivity of [C n mim][(CF3SO2) 2N] and [C4mim][BF4] IoNanofluids with Carbon Nanotubes—Measurement, Theory and Structural Characterization. Journal of Nanofluids. 2013;2(1):55-62.
59. Paul TC, Morshed AM, Khan JA. Nanoparticle Enhanced Ionic Liquids (NEILS) as working fluid for the next generation solar collector. Procedia Engineering. 2013;56:631-6.
60. Xuan Y, Li Q. Investigation on convective heat transfer and flow features of nanofluids. Journal of Heat transfer. 2003;125(1):151-5.
61. Xuan Y, Li Q. Heat transfer enhancement of nanofluids. International Journal of heat and fluid flow. 2000;21(1):58-64.
62. Chereches EI, Sharma KV, Minea AA. A numerical approach in describing ionanofluids behavior in laminar and turbulent flow. Continuum Mechanics and Thermodynamics. 2018;30(3):657-66.

List of Tables

Table 1. Properties of [Mmim][DMP] [19].

Property	Value
Purity (HPLC)	≥98.0%
Identity (NMR)	Passed
Density	1.27 g cm^{-3} (20 °C)
Water (KF)	≤0.1%
Halides (IC)	≤0.1%
Color	Yellow

Table 2. Thermophysical properties of Ti_3C_2 nanoparticle [19].

Property	value
Color	Black
Shape	2-D
Size	Thickness = 1 (nm) Lateral size = 1-10 (μm)
Purity (%)	≥ 99.998
Density/kg m^{-3}	3700
c_p /J kg^{-1} K^{-1}	2800

Table 3. Empirical correlations obtained from IL and INf experimental properties [19].

Correlations	R^2	AREP (%)
$\rho_{bf} = -284.05 + 9.0412T - 0.01547T^2$	0.9996	0.021
$C_{p,bf} = 3810.47 - 12.87T + 0.02434T^2$	0.994	0.086
$\mu_{bf} = 37.29 - 0.2031T + 0.0002905T^2$	0.997	0.66
$k_{bf} = 119.57 - 1.14151T + 0.003633T^2 - 3.8381E-06T^3$	1	0.24
$\rho_{nf} = 1201.34 - 0.4421T - 7139350\varphi^2 - 1.43E-05\frac{T^2}{\varphi^{0.28}}$	0.971	0.58
$C_{p,nf} = 576.42 + 2.71E05\varphi + 1.65E08\varphi^2 + 7.7T - 7.5E-03T^2$	0.981	0.42
$\mu_{nf} = (1.06 + 150.18f - 120000f^2)\mu_{bf}$	0.992	1.87
$k_{nf} = (-36.23 - 731.46f - 1.592E-04T^2 + (\frac{T}{k_{np}}) + 20.25(\frac{\mu_{nf}}{\mu_{bf}}))k_{bf}$	0.993	0.866

Table 4. Grid validation of computational geometry.

Face division	Nu_{avg}	Error (%)
1*250	7.909078	50.64
2*500	5.250143	4.60
3*750	5.018672	3.10
4*1000	4.869359	1.65
5*2000	4.790411	0.96
6*3000	4.744649	0.61
7*4000	4.715996	-

Table 5: The summary of the significant parameters.

Np	Base fluid	Thermophysical properties	Temperature	*Re*	Nf's concentration
Ti_3C_2	0.2 [Mmim][DMP]+ 0.8 water	Temperature-dependent	298.15-308.15 (K)	1-50	0.0-0.2 (wt.%)

Table 6: Comparison between previous studies and this work for the HTE of INfs.

Base fluid	Nanoparticle	NF's concentration (wt%)	HTE (%)	Ref.
0.2 [Mmim][DMP] IL + 0.8 water	Mxene	0.05	19.0	This study
		0.1	35.9	
		0.2	43.6	
0.25 $[C_2mim][CH_3SO_3]$ IL + 0.75 water	Al_2O_3	1	12.1	[13]
		2.5	13.9	
		5	23.3	
		10	32.7	
		15	50.0	
$[C_4mpyrr][NTf_2]$	Al_2O_3	2.5	- 22.2	[12]
[EMIM][EtSO4]	Al_2O_3	0.5	44.9	[14]
		1.0	12.3	
		2.5	5.7	
$[C_4mim][NTf_2]$	Al_2O_3	0.18	64.4	[6]
		0.36	85.0	

		0.9	125.2	
$[C_4mim][NTf_2]$	MWCNT	1.0	11.0	[6]
$[C_2mim][EtSO_4]$	MWCNT	1.0	9.0	[6]
[Hmim][BF4]	MWCNT	0.03	1.7	[6]
		0.06	10.0	
[Hmim][BF4]	Graphene	0.03	6.0	[6]
		0.06	12.1	

List of Figures

Figure 17. Validation of the developed equation [Eq. (9)] for Nusselt numbers with this work results.

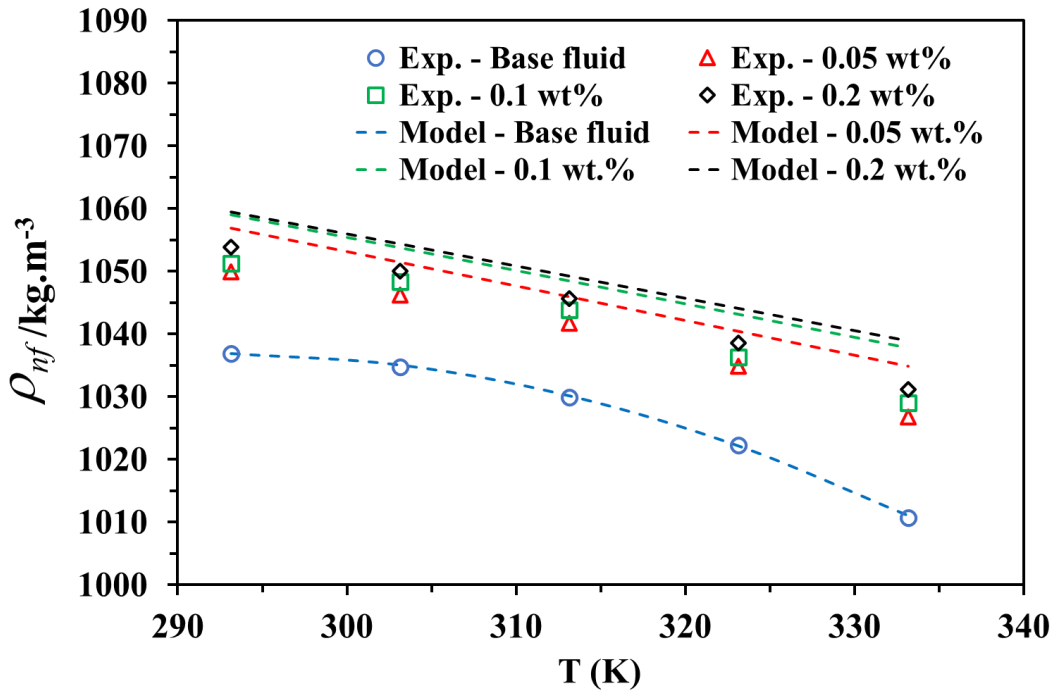

Figure (1). The comparison between the experimental measured density [19] and obtained empirical correlations.

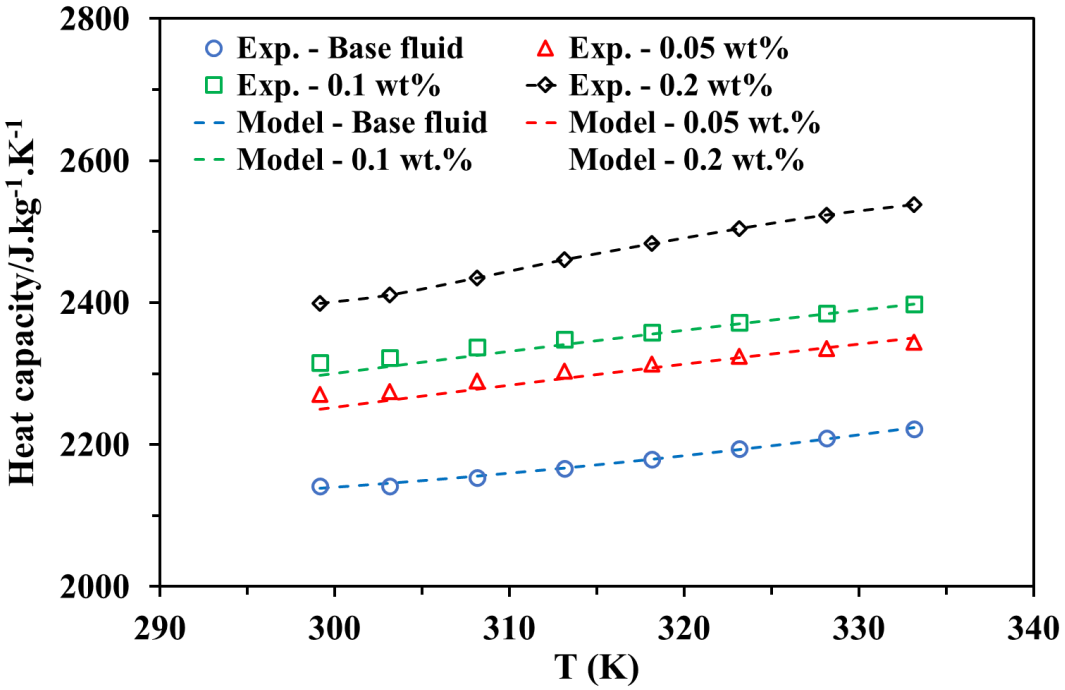

Figure (2). The comparison between the experimental measured heat capacity [19] and obtained empirical correlations.

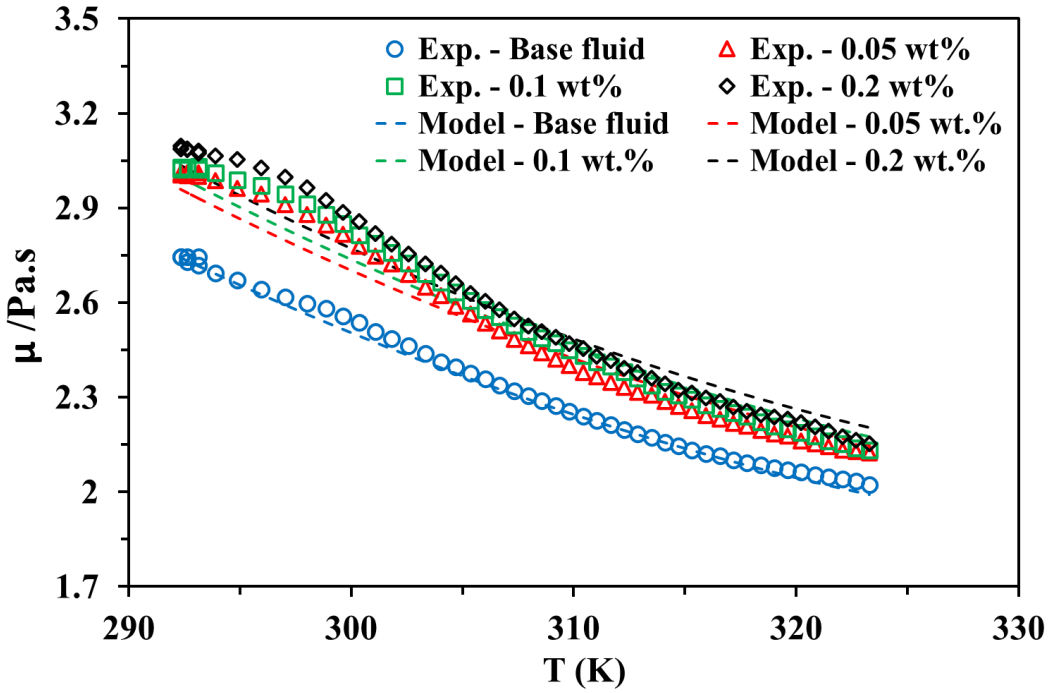

Figure (3). The comparison between the experimental measured viscosity [19] and obtained empirical correlations.

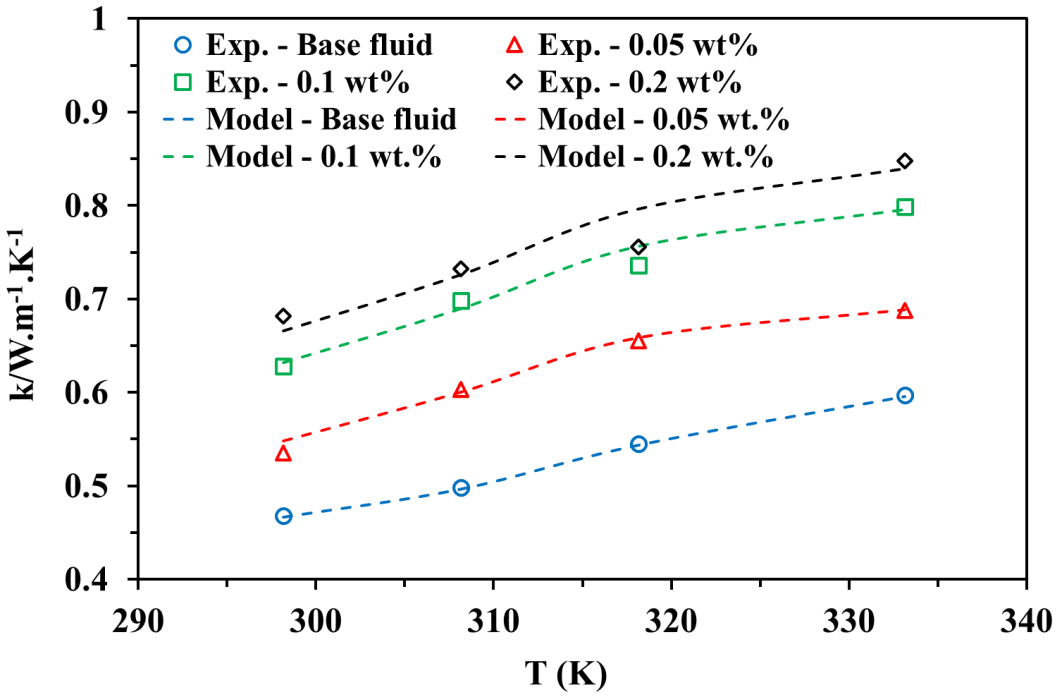

Figure (4). The comparison between the experimental measured thermal conductivity [19] and obtained empirical correlations.

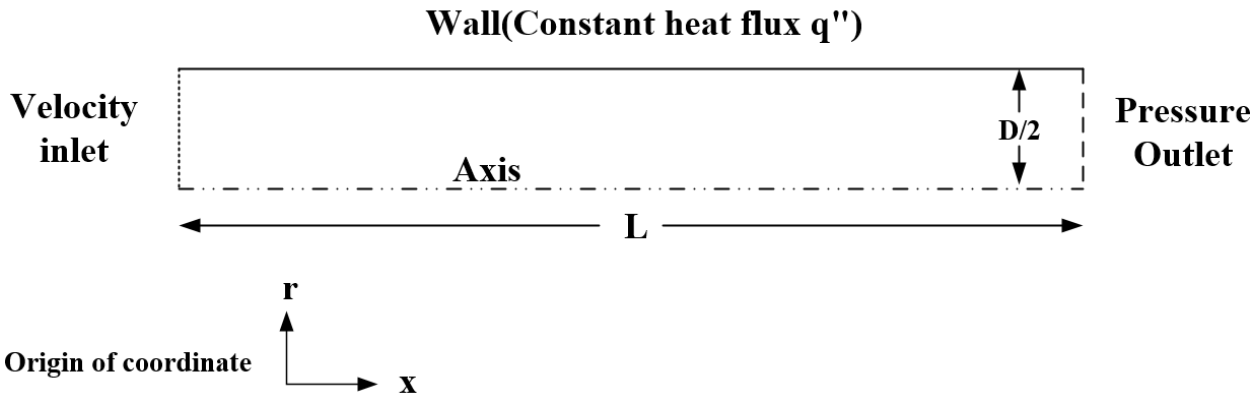

Figure 5. Computational model of the studied problem.

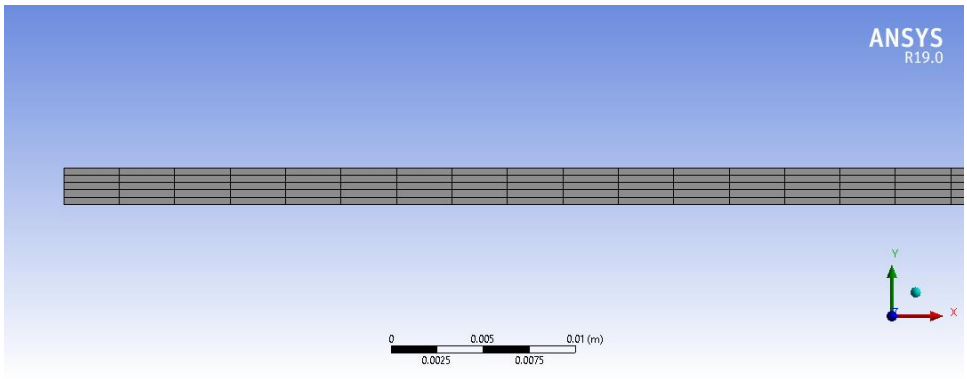

Figure 6. Mesh generated for the computational domain.

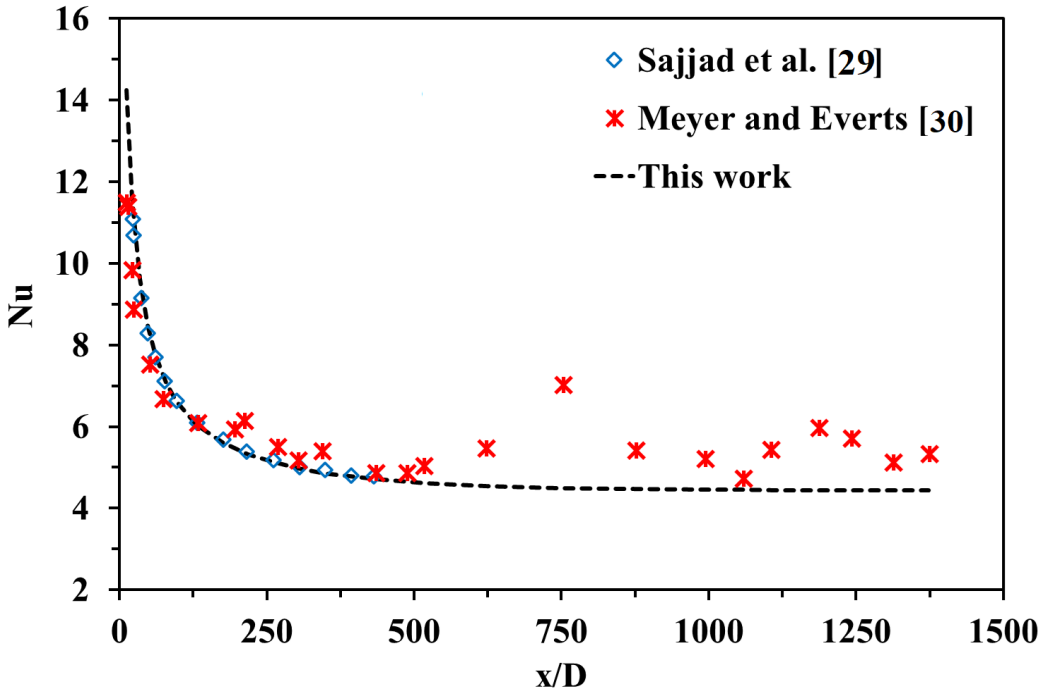

Figure 7. Validation of the studied problem with experimental and numerical works.

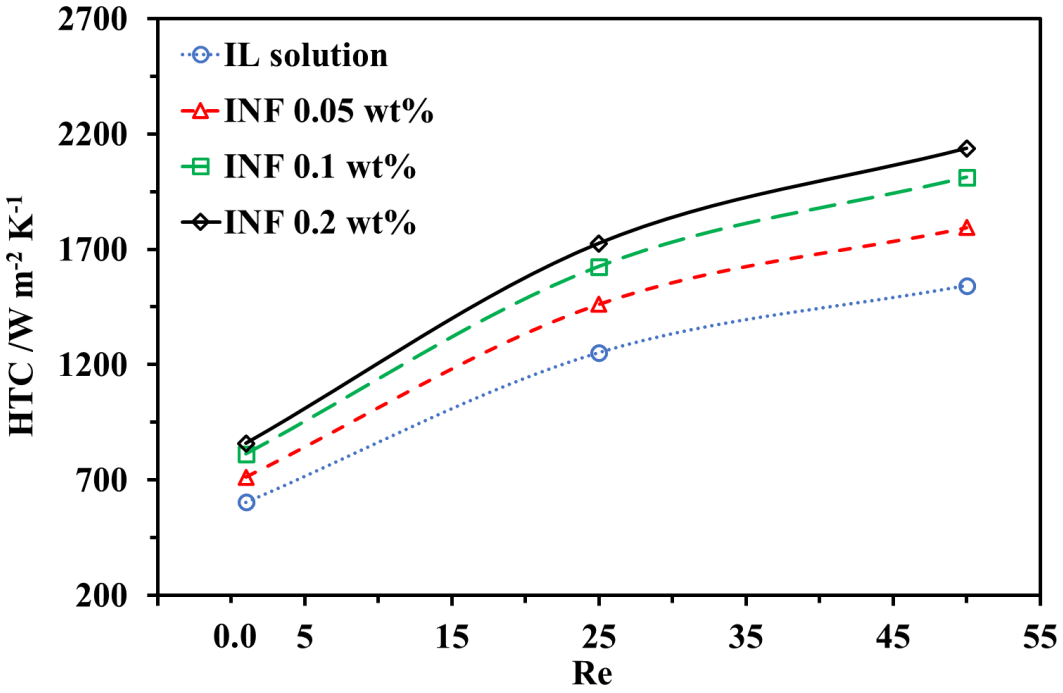

Figure 8. HTC vs. *Re* number for various concentrations of Nfs at T=298.15 K.

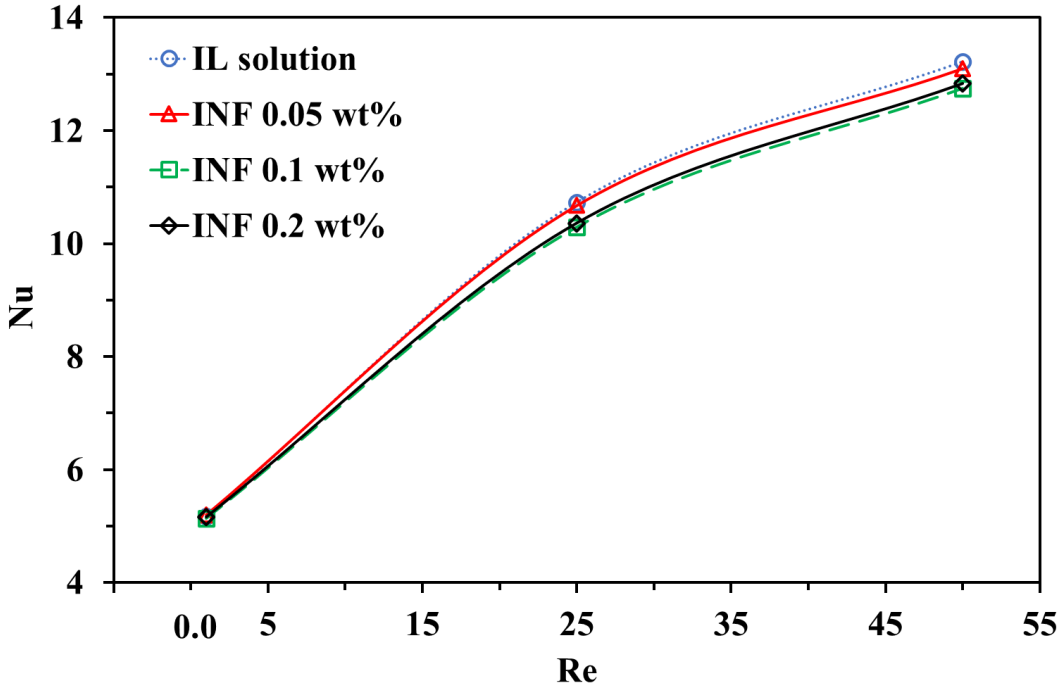

Figure 9. *Nu* vs. *Re* number for various concentrations of Nfs at T=298.15 K.

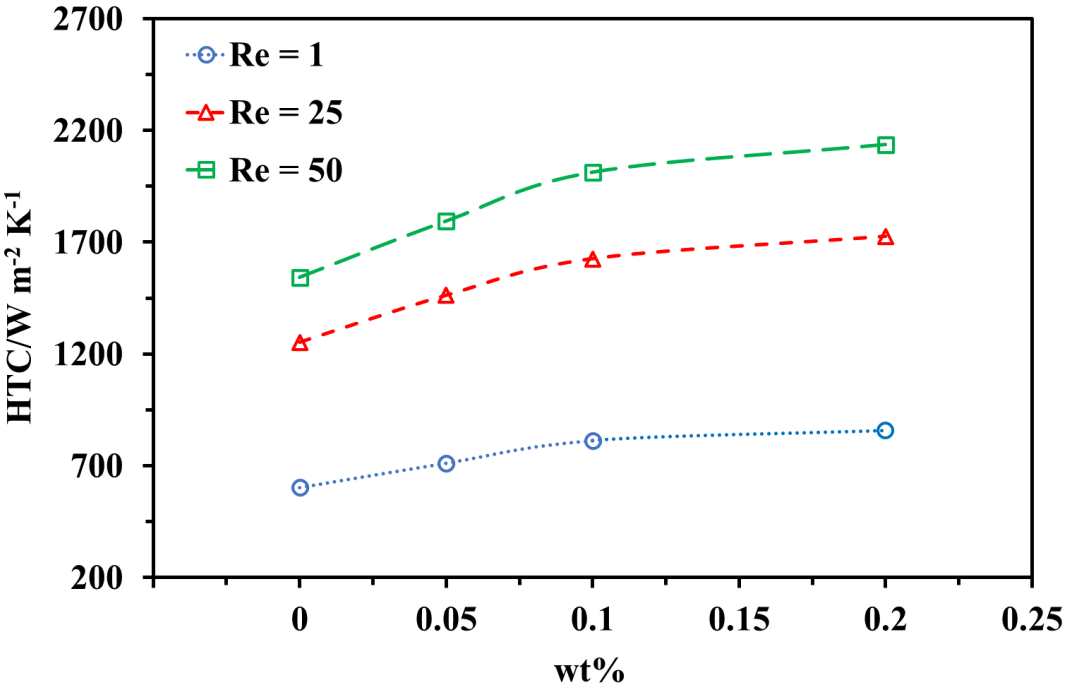

Figure 10. HTC vs. Nfs concentration for various *Re* numbers at T=298.15 K.

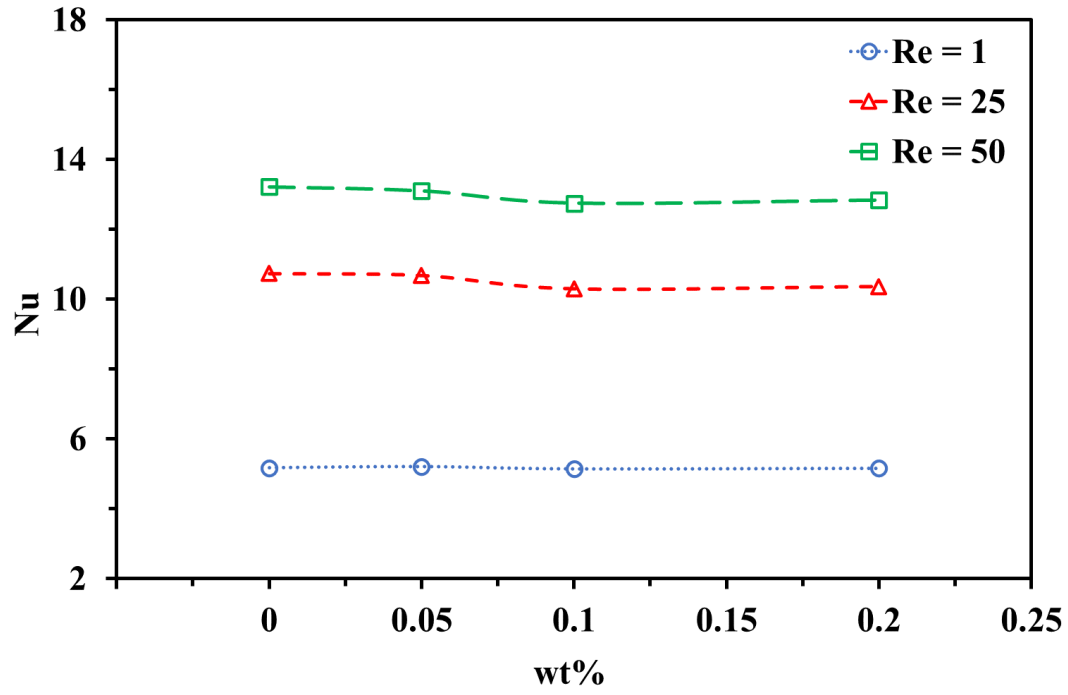

Figure 11. *Nu* vs. Nfs concentration for various *Re* numbers at T=298.15 K.

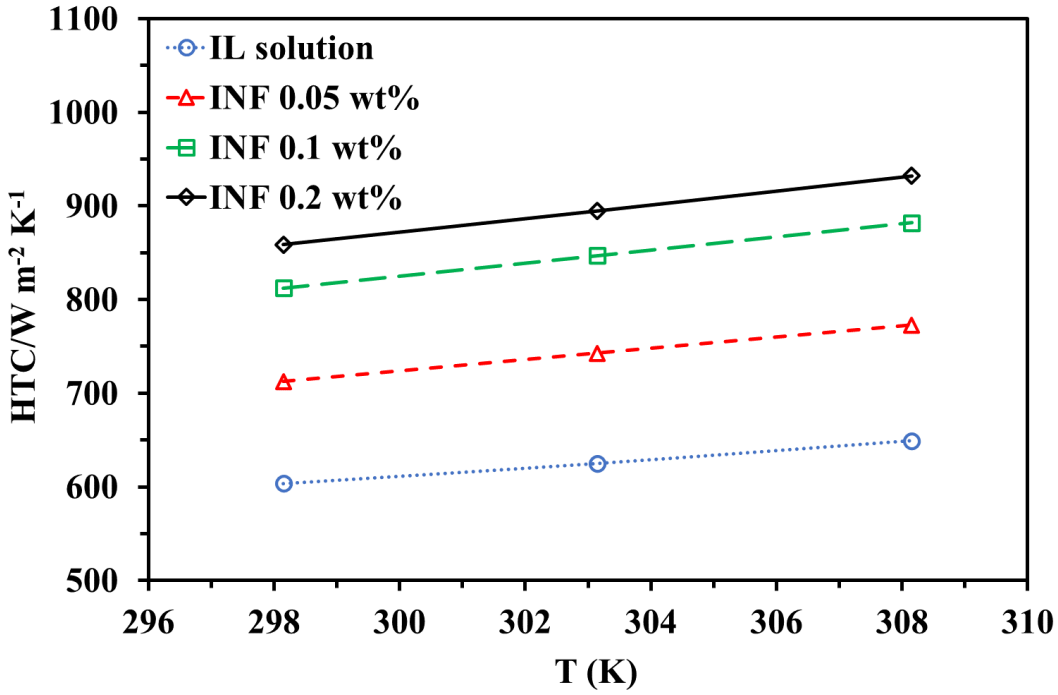

Figure 12. HTC vs. fluid inlet temperature for various Nfs at *Re* = 25.

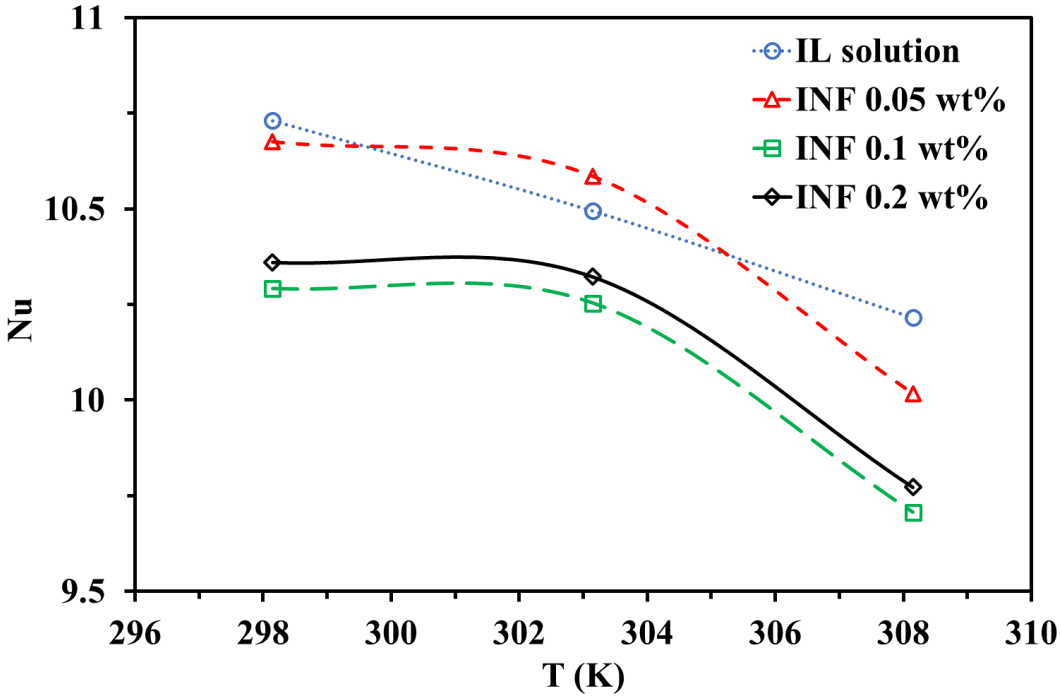

Figure 13. *Nu* vs. fluid inlet temperature for various Nfs at *Re* = 25.

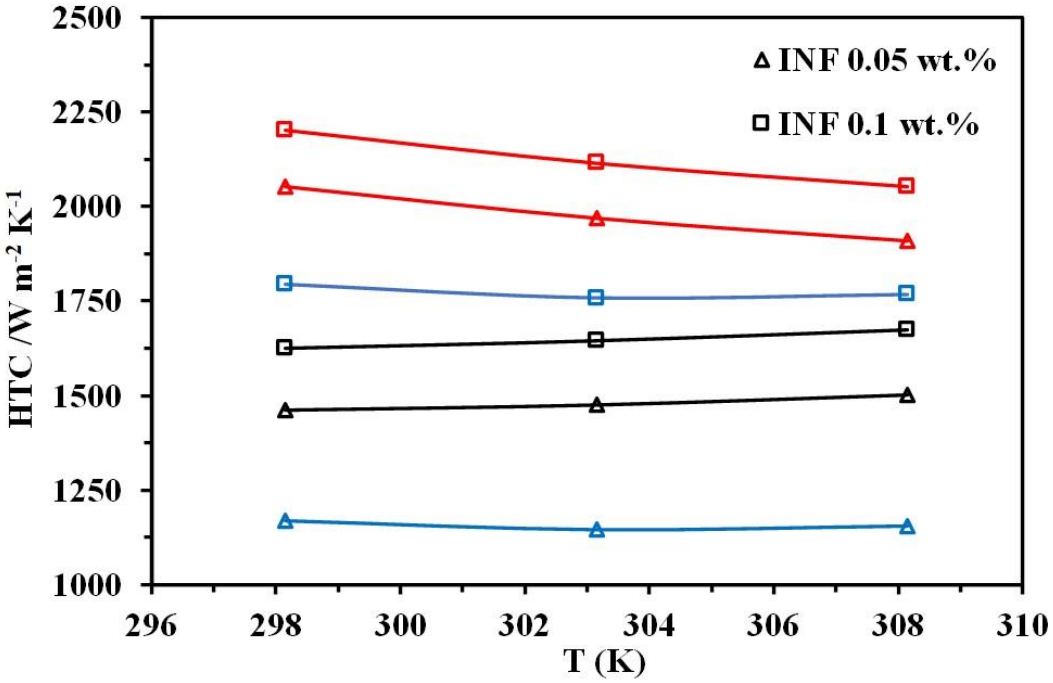

Figure 14. Comparison **of** HTC values calculated from Eqs. (4), (10), and (15) at *Re* = 25. (black line: **Eq. (4)** - blue line: **Eq. (10)** - red line: **Eq. (15)**).

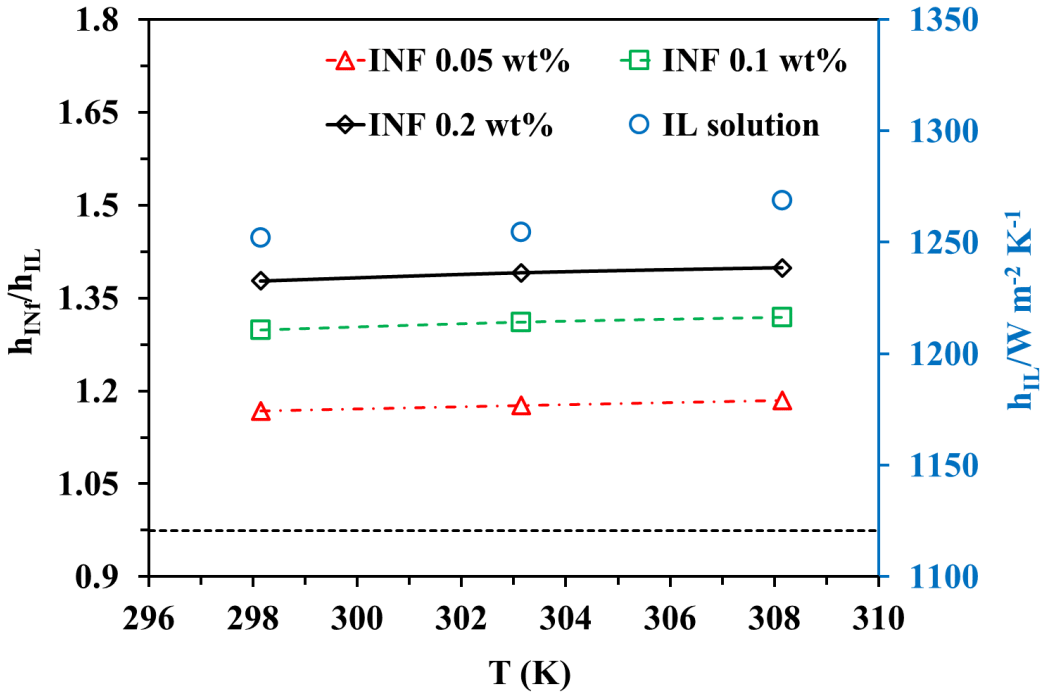

Figure 14. HTE vs. fluid inlet temperature for various volume fractions at Re = 25.

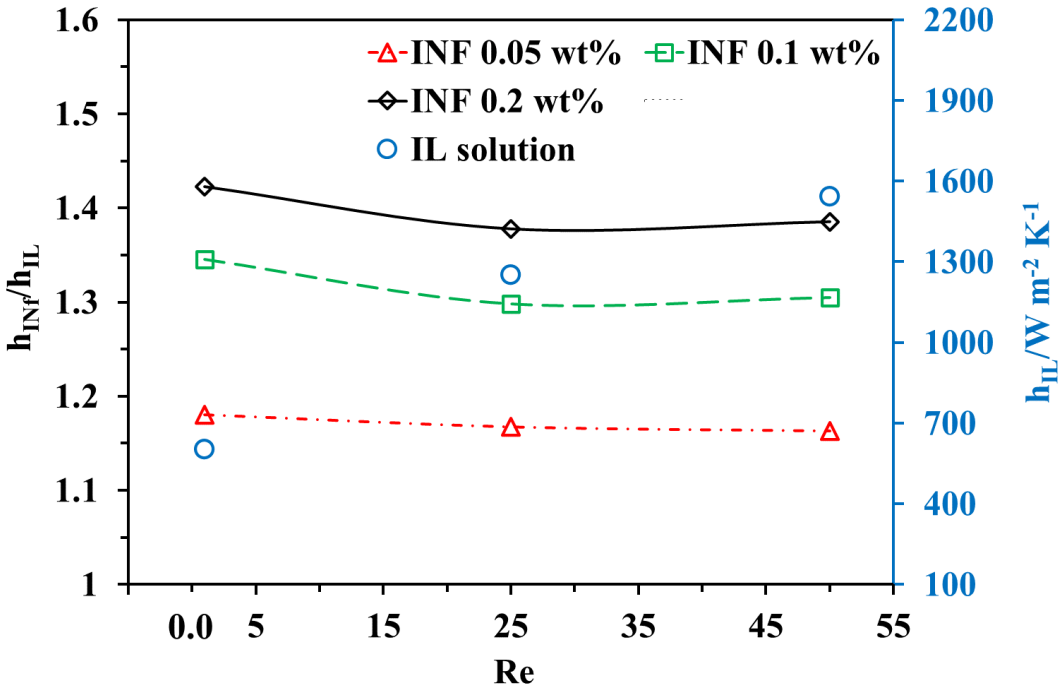

Figure 15. HTE vs. *Re* numbers for various volume fractions at T = 298.15 K.

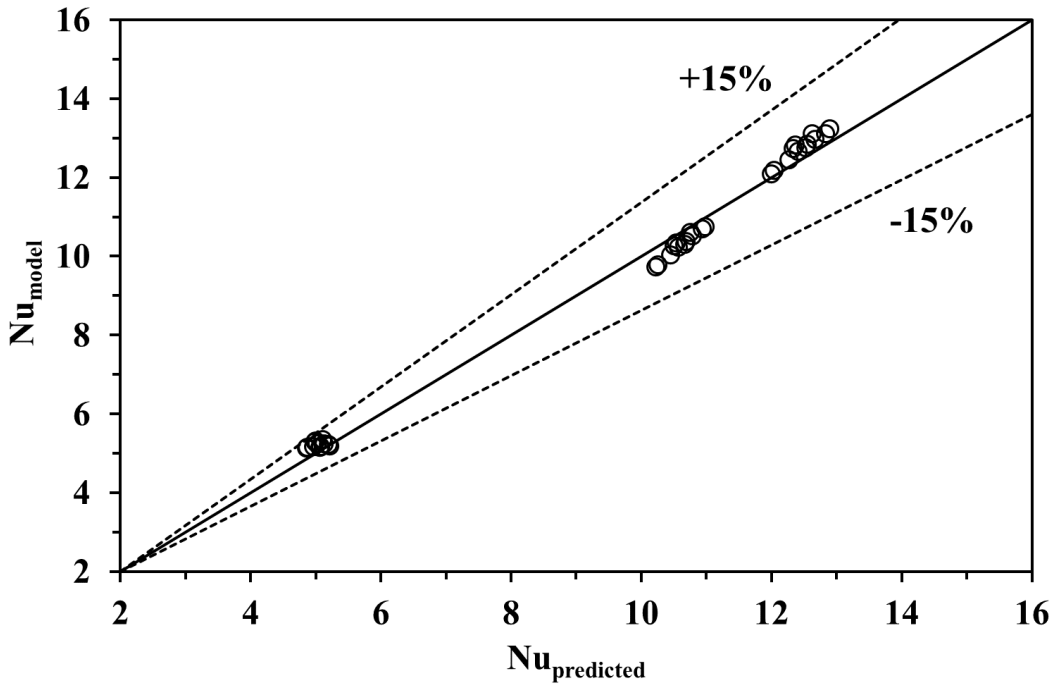

Figure 16. Validation of the developed equation [Eq. (11)] for Nusselt numbers with this work results.